ELSEVIER

Biophysical Chemistry 56 (1995) 129–135

Biophysical Chemistry

Vibrational spectra of room-temperature rhodopsin: concentration dependence in picosecond resonance coherent anti-Stokes Raman scattering

A. Popp, L. Ujj, G.H. Atkinson *

Department of Chemistry and Optical Science Center, University of Arizona, Tucson, AZ 85721, USA

Abstract

The vibrational degrees of freedom of room-temperature rhodopsin (Rh^{RT}), the central trans-membrane protein in vision, are measured at room temperature by picosecond resonance coherent anti-Stokes Raman scattering (PR/CARS). High signal-to-noise PR/CARS data for the ethylenic stretching, Schiff base, and hydrogen-out-of-plane modes of the retinal chromophore are quantitatively analyzed via third-order susceptibility relationships. The accurate determination of spectral features permit the PR/CARS bandshapes to be analyzed as a function of Rh^{RT} concentration, an essential factor in using picosecond time-resolved CARS techniques to measure the vibrational spectroscopy of picosecond intermediates in the Rh^{RT} photosequence. Of particular importance is the recognition that PR/CARS bandshapes are sensitive functions of both the chromophore concentration and the excitation wavelength, as measured relative to the absorption spectra of specific chromophores (static and transient).

Keywords: Rhodopsin; Raman; Vision; Picosecond spectroscopy; Coherent spectroscopy

1. Introduction

The importance of photo-sequence the room-temperature rhodopsin (Rh^{RT}) photosequence in the energy storage/transduction mechanism underlying vision has been long established [1–3]. The kinetic properties of the Rh^{RT} photo-sequence have been determined largely from studies using time-resolved absorption spectroscopy in which a variety of intermediates have been identified [3–7]. Although it is known that the major part of the absorbed photon energy is stored in the batho-rhodopsin intermediate [1], the precise kinetics associated with batho at room temperature ($batho^{RT}$) remain under examination [4,6,7]. For example, a recent picosecond transient absorption study clarified the $batho^{RT}$ formation from photo-rhodopsin ($photo^{RT}$) by demonstrating $photo^{RT} \rightarrow batho^{RT}$ occurs with a 5 ± 1-ps time constant [8]. $Batho^{RT}$ subsequently forms an equilibrium with a blue-shifted intermediate (BSI) on the nanosecond time scale while BSI subsequently decays to lumi-rhodopsin which is followed by the meta-rhodopsin intermediates (meta I, II, and III). Seconds after excitation of Rh^{RT}, only meta II, free *all-trans* retinal and opsin are present. Transduction of the absorbed energy into a nerve signal occurs

* Corresponding author.

SSDI 0301-4622(95)00024-0

only after in vivo signal amplification and alteration of lipid conformations in meta II [9,10].

The formation and decay dynamics as well as the structure of batho^{RT} are crucial for elucidating the energy storage/transduction process in vision. With one exception [11], the only vibrational information available for the early (e.g., batho) intermediates in the Rh^{RT} photo-sequence has been obtained via infrared absorption and resonance Raman (RR) scattering from samples at temperatures low enough to trap (i.e., stabilize) a specific Rh intermediate [12–17]. Vibrational data recorded at such low temperatures (including that from batho^{LT}), as well as the mechanistic models based on them, may not accurately represent the structural changes occurring in the room-temperature Rh photo-sequence. This potential inconsistency is apparent when the molecular basis for thermally trapping a Rh intermediate is considered. Thermal interruption of the Rh photo-sequence occurs because the protein environment in which the retinal chromophore changes structurally prevents transformations between specific intermediates. The precise molecular mechanism(s) underlying these thermally-dependent protein barriers remains to be determined, but they may arise through the loss of structural flexibility and/or by changes in electrostatic properties that affect the retinal. Independent of the mechanism, the protein environment at low temperature experienced by the retinal chromophore is effectively different than that at room temperature. These differences are well recognized in the case of photointermediates in the related retinal protein, especially for the K-590 intermediate bacteriorhodopsin [18]).

Since the protein environment itself plays a significant role(s) in the energy storage/transduction mechanism of the Rh photo-sequence, it is not surprising that vibrational data recorded at temperatures low enough to trap Rh intermediate do not agree with vibrational data recorded directly from the Rh^{RT} photo-sequence. The dilemma has been that vibrational data from Rh^{RT} intermediates are experimentally difficult to obtain. These experimental limitations have recently been removed in studies based on picosecond time-resolved coherent anti-Stokes Raman scattering (PTR/CARS) [19]. PTR/CARS spectra recorded from the Rh^{RT} photo-sequence have shown the vibrational bands assigned to the C=C stretching modes of batho^{RT} and batho^{LT} differ significantly (by > 5 cm^{-1} [19]). Vibrational features in other regions of the PTR/CARS spectra from batho^{RT} agree well with those reported in the RR spectra from batho^{LT}, but the differences observed alter the interpretation of the Rh energy storage/transduction mechanism [19].

Quantitative $\chi^{(3)}$ analyses of PTR/CARS data require a detailed understanding of the picosecond resonance coherent anti-Stokes spectroscopy (PR/CARS) of stable, ground-state Rh^{RT} including the effects of Rh^{RT} concentration on PR/CARS features. For example, time-dependent structural changes in retinal that accompany the Rh^{RT} to batho^{RT} transformation can be extracted from the PTR/CARS data only if the concentration dependence of PR/CARS signals from Rh^{RT} is quantitatively known. Structural data acquired under these physiological conditions (temperatures) significantly improve our understanding of the molecular processes involved in vision.

2. Experimental and analysis

Bovine rhodopsin samples are isolated and purified following established procedures [20]. The instrumentation and experimental procedure used to record PR/CARS data from a photostable species, as well as the general third-order susceptibility ($\chi^{(3)}$) analysis used to interpret PR/CARS data, are presented elsewhere [21]. Those aspects of the $\chi^{(3)}$ analysis pertaining to the effect(s) of chromophore concentration in the interpretation of these PR/CARS data are described here.

PR/CARS data contain both resonant ($\chi^{(3)}_{VR}$) and non-resonant ($\chi^{(3)}_{NR}$) contributions from the retinal chromophore and water/protein, respectively [21]. Specifically, the PR/CARS signal (I_a) is proportional to the absolute square of $\chi^{(3)}(\omega_a, \omega_1, \omega_1, -\omega_s)$. In this work, $\omega_1 = 569$ nm and $\omega_s = 623 \pm 5$ nm or $\omega_s = 600 \pm 5$ nm are used to record PR/CARS date in the C=C-stretch/Schiff base or hydrogen-out-of-plane (HOOP) regions, respectively. Both ω_1 and ω_a ($= 2\omega_1 - \omega_s$) are in electronic resonance with the retinal chromophore in Rh^{RT}, but not with either the water solvent or the protein. The CARS spectrum of Rh^{RT} can be obtained by dividing the

measured PR/CARS signal from the sample (I_a) by the CARS signal measured from water alone (I_a^{water}). This procedure also removes instrumental responses.

The energies of the two PR/CARS probe pulses (8-ps durations) at 569 nm (< 1 nJ) and at 623 ± 5 nm or 600 ± 5 nm (2 nJ) are selected to be small enough (< 3% excitation) to minimize photochemical/photophysical perturbations that alter the reaction mixture present at a given time delay [22], but which optimize for high signal-to-noise ratio (S/N). For a sample at a given Rh^{RT} concentration, the ratio of $\chi^{(3)}$ from the sample and $\chi^{(3)}_{NR}$ is:

$$\left|\frac{\chi^{(3)}}{\chi^{(3)}_{NR}}\right|^2 \propto \frac{I_a}{I_a^{water}} = \mu^2\left|1+\gamma\frac{\chi^{(3)}_{VR}(Rh)}{\chi^{(3)}_{NR}}\right|^2;$$

$$\frac{\chi^{(3)}_{VR}(Rh)}{\chi^{(3)}_{NR}} = e^{i\theta}\sum_{j=1}^{N}\frac{A_j}{-\delta_j - i};\ \delta_j = \frac{\Omega_j - (\omega_1 - \omega_s)}{\Gamma_j} \quad (1)$$

where Ω_j is the j^{th} vibrational frequency of Rh^{RT} having a bandwidth Γ_j (HWHM) and $e^{i\theta}A_j$ is the complex amplitude of the j^{th} oscillator strength. The μ^2 term can be considered a scaling factor and γ is the actual concentration of the chromophore.

The Rh^{RT} sample is examined as a free-flowing, liquid jet at ca. 10° C. The sample speed is adjusted to ensure that each successive pair of laser pulses examines new material. With an excitation volume of ca. 10^{-7} ml, a total sample volume of ca. 10 ml and a laser repetition rate of 400 kHz, the mean time interval between when the same Rh^{RT} volume is probed via PR/CARS is several minutes. Within several minutes, the originally excited Rh^{RT} has formed meta II and/or free retinal and opsin (vide supra). These latter species all have absorption maxima of ≤ 380 nm and therefore, are not resonantly enhanced by either ω_1 or ω_a (≥ 520 nm, vide supra). Nonetheless, the accumulation time for each PR/CARS spectrum is selected to be only 30 s and the spectra are averaged only long enough to ensure that no spectral changes appear. The spectra shown in Figs. 1 and 2 are averages of 4 to 6 PR/CARS spectra each recorded for 30 s. Thus the Rh^{RT} sample is exposed for only a few minutes during each measurement to obtain vibrational spectra of excellent S/N (Figs. 1 and 2).

Compared to spontaneous resonance Raman (RR), the PR/CARS methodology offers several important experimental advantage for use with Rh^{RT}:

(1) The measured S/N is significantly increased because the PR/CARS signal can be detected as a spatially separated, coherent beam and unlike RR scattering, no signal is lost due to a finite optical collection efficiency.

(2) Fluorescence, which normally exceeds the RR signal, does not interfere with the PR/CARS signal at all.

(3) The intensity of the CARS signal is proportional to the intensity of the broadband ω_s beam [21], which can be relatively intense if ω_s does not overlap the absorption spectrum of the chromophore.

3. Results and discussion

PR/CARS data recorded at different concentrations of Rh^{RT} are presented for the C=NH^+ and ethylenic-stretching modes (1460–1700 cm^{-1}) in Fig. 1 while the corresponding PR/CARS data for the HOOP (760–1050 cm^{-1}) region are shown in Fig. 2. Fits based on $\chi^{(3)}$ analyses (Eq. 1) of these PR/CARS data are also presented in Figs. 1 and 2. The resultant origins, bandwidths (HMHW), and amplitudes for Rh^{RT} are listed in Table 1.

The dispersive appearance of the PR/CARS data from Rh^{RT} (Figs. 1 and 2) is due to: (i) the resonance enhancement of CARS at ω_1 and ω_a on the red side of the absorption band of Rh^{RT} and (ii) the relatively large contribution of $\chi^{(3)}_{NR}$ to the total PR/CARS signal [23,24]. When the contribution of $\chi^{(3)}_{VR}$ (γ) is large, (i.e. the chromophore concentration is large), the PR/CARS bandshapes become Lorentzian, [21–25]. Changes in the band appearance due to the concentration dependence of PR/CARS (Figs. 1a–d and 2a–d) are due only to altering the value of γ (i.e., $\chi^{(3)}_{VR}$ relative to $\chi^{(3)}_{NR}$, Eq. 1).

All PR/CARS spectra of Rh^{RT} are fit with one set of parameters and only γ is permitted to vary. The band origins and bandwidths are kept constant within < 1 cm^{-1} except for the weak 1626 cm^{-1} and 1035 cm^{-1} features where a variation of < 2 cm^{-1} is used to achieve an acceptable (< 7.5%) $\chi^{(3)}$ fit.

Only five bands (1545 cm^{-1}, 1577 cm^{-1}, 1601 cm^{-1}, 1626 cm^{-1} and 1653 cm^{-1}) are used in the fitting procedure for the C=C stretch/Schiff base region (Fig. 1). A broad (Γ ca. 15 cm^{-1}), weak (A ca. 0.07) band at ca. 1445 cm^{-1} is introduced to complete the $\chi^{(3)}$ analysis on the low-wavenumber side. Residuals (ρ) describing the error of the $\chi^{(3)}$ fit contain only high-frequency noise ($\pm 7.5\%$ over 1480 to 1680 cm^{-1}). A small modulation of the ρ-function in the region of the most intense C=C-stretch vibration is observed. The corresponding normal mode is broad and is assigned as a symmetric

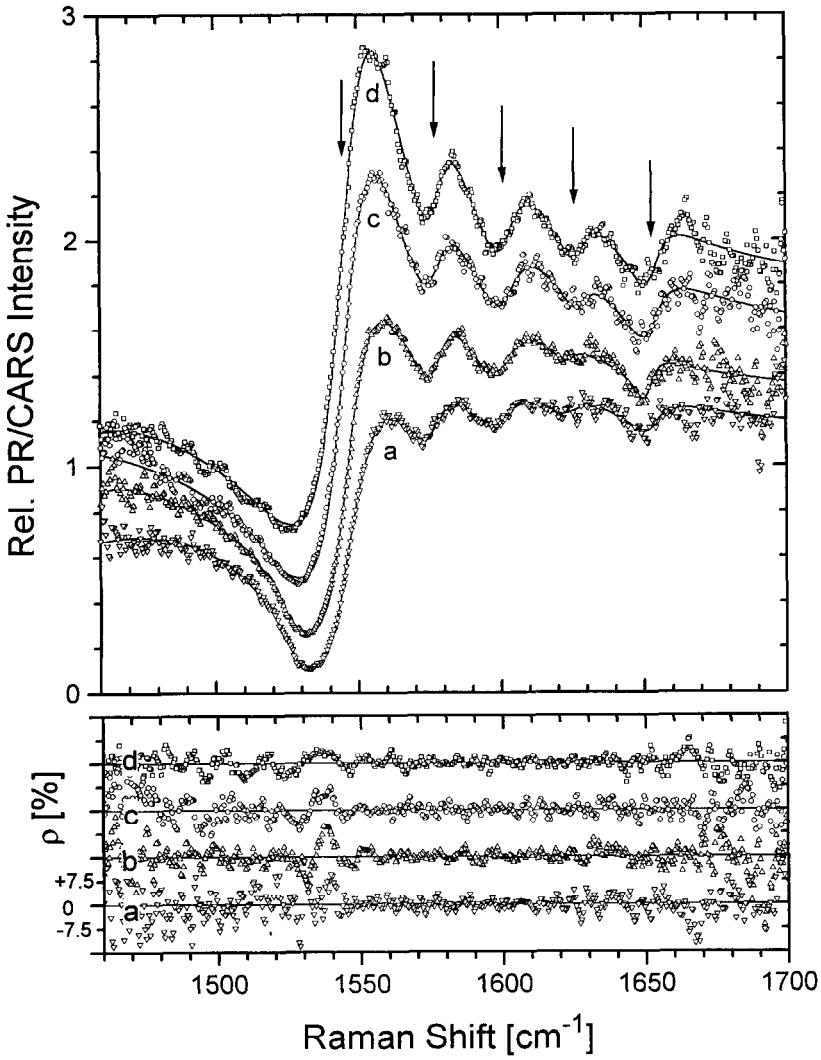

Fig. 1. Upper panel: the picosecond resonance CARS (PR/CARS) spectra of the C=C stretching and C=NH^+ modes (1460 cm^{-1} – 1700 cm^{-1} region) of room-temperature rhodopsin (Rh^{RT}) at different concentrations (a: $OD_{498} = 3.2$, b: $OD_{498} = 2.8$, c: $OD_{498} = 2.4$, and d: $OD_{498} = 1.4$) together with their respective fits based on $\chi^{(3)}$-analyses. The spectra b, c, and d are displaced from spectrum a by 0.2, 0.4 and 0.6, respectively, to facilitate comparisons. The band origin positions for features assigned to Rh^{RT} are derived from a $\chi^{(3)}$ analysis (Eq. 1). The positions of all bands indicated by vertical arrows are presented in Table 1. Lower panel: the residual function, ρ (i.e., difference between PR/CARS data and a fit based on $\chi^{(3)}$-analyses, normalized to the PR/CARS data) for the spectra a–d. Error limits of $\pm 7.5\%$ are also indicated.

C=C stretching vibration [16]. Consistent with this observation is the appearance of a vibrational band composed of at least two different, strongly overlapping vibrational modes. Analogous modes are found from a PR/CARS study of bacteriorhodopsin [21,25].

In the HOOP region (Fig. 2), all PR/CARS spectra are fit with seven bands: 799 cm^{-1}, 844 cm^{-1}, 970 cm^{-1}, 976 cm^{-1}, 999 cm^{-1}, 1020 cm^{-1}, and 1035 cm^{-1}. Two overlapping bands near 970 cm^{-1} must be introduced to reproduce the observed

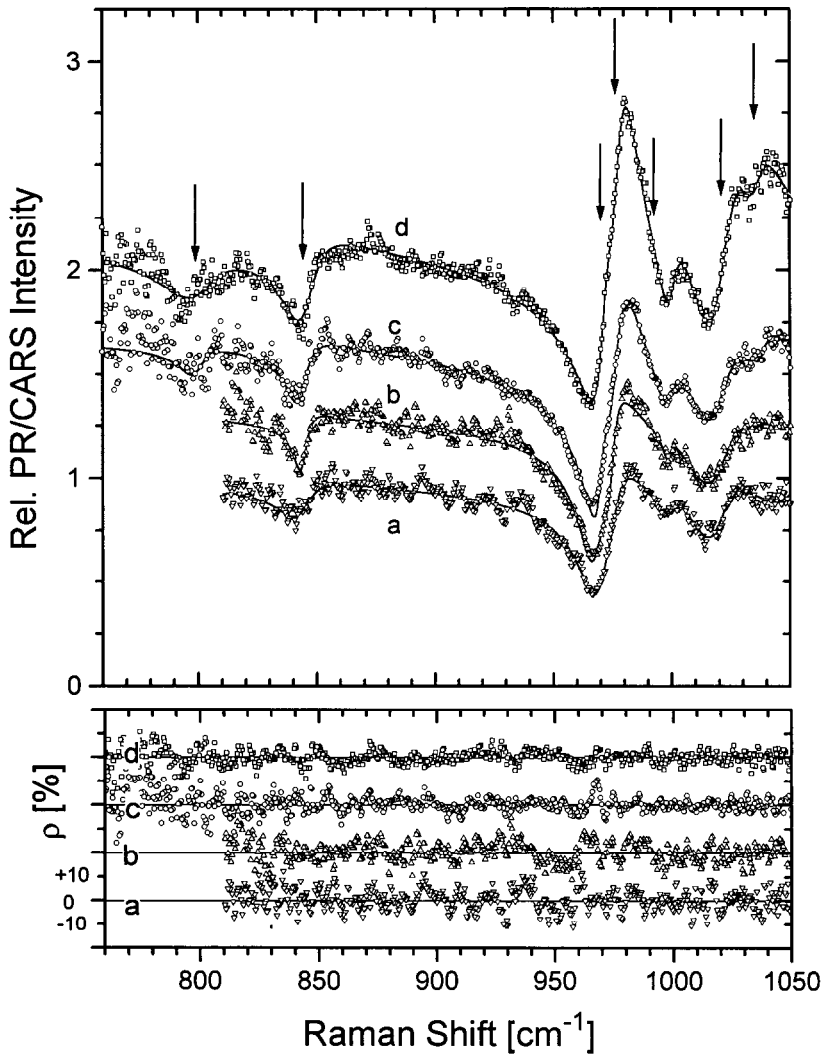

Fig. 2. Upper panel: the picosecond resonance CARS (PR/CARS) spectra of hydrogen-out-of-plane (HOOP) modes (760 cm^{-1}–1050 cm^{-1} region) of room-temperature rhodopsin (Rh^{RT}) at different concentrations (a: $OD_{498} = 3.5$, b: $OD_{498} = 2.5$, c: $OD_{498} = 1.5$, and d: $OD_{498} = 1.0$) together with their respective fits based on $\chi^{(3)}$-analyses. The spectra b, c, and d are displaced from spectrum a by 0.5, 0.75 and 1.25, respectively, to facilitate comparisons. The band origin positions for features assigned to Rh^{RT} are derived from a $\chi^{(3)}$ analysis (Eq. 1). The positions of all bands indicated by vertical arrows are presented in Table 1. The PR/CARS spectra at low Rh^{RT} concentrations (a and b) are shown in the region from 810 cm^{-1} to 1050 cm^{-1} due to the poor S/N on the low-wavenumber side. Lower panel: the residual function, ρ (i.e., difference between PR/CARS data and a fit based on $\chi^{(3)}$-analyses, normalized to the PR/CARS data) for the spectra a–d. Error limits of $\pm 10\%$ are also indicated.

Table 1
Comparison of the vibrational data for rhodopsin obtained by PR/CARS and resonance Raman (RR) scattering. Band origin positions (Ω), band widths (Γ) and relative amplitudes (A) are obtained by fitting the HOOP and C=C stretching regions of the PR/CARS spectra of rhodopsin at room temperature to a $\chi^{(3)}$ relationship (Eq. 1). The amplitudes are normalized for both spectral regions to the most intense bands (970 cm^{-1} and 1545 cm^{-1}, respectively). The phase is $131 \pm 3°$ for the HOOP region and $122 \pm 3°$ for the C=C region. The intensity maxima positions for Rh^{LT} and Rh^{RT} as measured by RR spectroscopy (excitation wavelength is given in nm) are presented to facilitate comparisons. The values of ω_i/ω_s are given for the PR/CARS data

Resonance Raman						PR/CARS		
Rh^{LT}		Rh^{RT}				Rh^{RT}		
482 [12]	488 [16]	600 [26]	590 [12]	488 [15]	458–647 [27]	568/600, 568/623		
Band maxima (cm^{-1})						Ω (cm^{-1})	Γ (cm^{-1})	A
					809 824	799	10	0.06
847	848	847	845		859	844	6	0.13
						970	5	0.60
970	970	971	970	971	970			1.00
						976	5	0.40
1000	1000	1000	999	998	999	999	5	0.09
						1020	10	0.27
1019	1019	1018	1016	1018	1018			
						1035	8	0.11
				1070		(1075)	(10)	
		1450		1435	1432 1442	(1443)	(20)	
1550	1549	1545	1545	1546	1549	1545	14	1.00
1583	1582	1580		1580	1581	1577	8	0.13
	1599							
1599		1605	1595	1607	1609	1602	9	0.10
	1609							
1634	1636		1633	1635		1627	6	0.04
1655	1657	1660	1655	1658	1659	1653	7	0.07

band shape. A broad, weak band at 1075 cm^{-1} is used at the high-wavenumber edge of these spectra (Fig. 2). The low-concentration spectra (Fig. 2a and b) are only displayed from 810 cm^{-1} to 1050 cm^{-1} because of the poor S/N on the low-wavenumber side. The corresponding ρ-functions contain only high-frequency noise ($\leq 10\%$ for 810 cm^{-1} to 1050 cm^{-1}).

The parameters obtained from the $\chi^{(3)}$ analyses are in good agreement with previously published RR results for Rh^{RT} (Table 1) [12,15,16,26,27]. Small deviations of RR band maxima and PR/CARS origin positions are attributable to congestion in the RR spectra where band origins and band maxima are difficult to distinguish.

There is no evidence that the meta intermediates, *all-trans* retinal, or opsin, all of which appear in the Rh^{RT} sample as excitation proceeds, contribute to the PR/CARS data reported. The PR/CARS data can be fit with the same parameter set by changing only γ (chromophore concentration). No additional bands must be included in the $\chi^{(3)}$ analysis.

It is evident from Figs. 1 and 2 that PR/CARS data monitored as a function of Rh^{RT} concentration can be quantitatively analyzed in terms of a $\chi^{(3)}$ relationship (Eq. 1). As a consequence, several conclusions can be reached:

(1) Comparison with spontaneous RR data from Rh^{RT} shows excellent agreement, confirming that the combined PR/CARS measurements and $\chi^{(3)}$ analysis provide an accurate characterization of the Rh^{RT} vibrational degrees of freedom.

(2) High S/N vibrational spectra can be recorded from the relatively small amounts (30 OD ml) of Rh^{RT} samples available from normal preparative procedures. PR/CARS data may, therefore, be obtained from artificial (i.e., modified retinal) and/or mutant Rh-samples where the amounts available are severely limited.

(3) Since no contributions from other species in

the Rh^{RT} photo-sequence are found in these PR/CARS data, essentially no optical perturbation of the Rh^{RT} photo-sequence occurs. Thus, the experimental conditions used here are appropriate for monitoring time-dependent concentrations of Rh^{RT} intermediates in PTR/CARS measurements. The bandshapes for the early Rh^{RT} photo-intermediates $photo^{RT}$ and $batho^{RT}$ are anticipated to be Lorentzian with phase of ca. 270° since their absorption maxima are near ω_1 and ω_a [23,24]. Such results would parallel those from related studies of bacteriorhodopsin intermediates [21,22,25]. Under these conditions, PTR/CARS data can be used to measure the vibrational degrees of freedom of each Rh^{RT} intermediate and thereby, provide direct information on structures of these species for the first time.

Acknowledgements

This work was supported by a grant to GHA from the National Institutes of Health. AP wishes to gratefully acknowledge support from the Alexander von Humboldt Foundation as a Feodor Lynen Scholar and from the University of Arizona Foundation.

References

[1] R.R. Birge, Ann. Rev. Phys. Chem., 41 (1990) 683.
[2] P. Hargrave, Curr. Opinions Struct. Biol., 1 (1991) 575.
[3] J.W. Lewis and D.S. Kliger, J. Bionerg. Biomembr., 24 (1992) 201.
[4] H. Kandori, S. Matuoka, Y. Shichida and T. Yoshizawa, Photochem. Photobiol., 49 (1990) 1179.
[5] C.E. Randall, J.W. Lewis, S.J. Hug, S.C. Björling, I. Eisner-Shanas, N. Friedman, M. Ottolenghi, M. Sheves and D.S. Kliger, J. Am. Chem. Soc., 113 (1991) 3473.
[6] M. Yan, D. Manor, G. Weng, H. Cao, L. Rothberg, T.M. Jedju, R.R. Alfano and R.H. Callender, Proc. Natl. Acad. Sci. USA, 88 (1991) 9809.
[7] L.A. Peteanu, R.W. Schoenlein, Q. Wang, R.A. Mathies and C.V. Shank, Proc. Acad. Natl. Sci. USA, 90 (1993) 11762.
[8] A. Popp, L. Ujj and G.H. Atkinson, J. Phys. Chem., submitted.
[9] W. DeGrip, D. Gray, J. Gillespie, P.M.H. Bovee, E.M.M. van den Berg, J. Lugtenburg and K.J. Rothschild, Photochem. Photobiol., 48 (1988) 497.
[10] N.J. Gibson and M.F. Brown, Biochemistry, 32 (1993) 2438.
[11] G. Hayward, W. Carlsen, A. Siegman and L. Stryer, Science, 211 (1981) 942.
[12] M.A. Marcus and A. Lewis, Photochem. Photobiol., 29 (1979) 699.
[13] G. Eyring and R. Mathies, Proc. Natl. Acad. Sci. USA, 76 (1979) 33.
[14] K.A. Bagley, V. Balogh-Nair, A.A. Croteau, G. Dollinger, T.G. Ebrey, L. Eisenstein, M.K. Hong, K. Nakanishi and J. Vittitow, Biochemistry, 24 (1985) 6055.
[15] I. Palings, J.A. Pardoen, E. van den Berg, C. Winkel, J. Lugtenburg and R. Mathies, Biochemistry, 26 (1987) 2544.
[16] H. Deng and R.C. Callender, Biochemistry, 26 (1987) 7418.
[17] P. Rath, L.L.J. Decaluwe, P.H.M. Boveegeurts, W.J. DeGrip and K.J. Rothschild, Biochemistry, 32 (1993) 10277.
[18] T. Kitagawa and A. Maeda, Photochem. Photobiol., 50 (1989) 883.
[19] A. Popp, L. Ujj and G.H. Atkinson in W. Knox and P. Barbara (Editors), Ultrafast Phenomena IX, Springer Verlag, Berlin, Vol. 60, 1994, p. 454.
[20] J.S. Horwitz, J.W. Lewis, M.A. Powers and D.S. Kliger, Photochem. Photobiol., 37 (1983) 181.
[21] L. Ujj, B.L. Volodin, A. Popp, J.K. Delaney and G.H. Atkinson, Chem. Phys., 182 (1994) 291.
[22] G.H. Atkinson, A. Popp and L. Ujj, in A. Lau, F. Siebert and W. Wernecke (Editors), Time Resolved Vibrational Spectroscopy VI, Springer Verlag, Berlin, 1994, pp. 153–157.
[23] J.L. Oudar and Y.R. Shen, Phys. Rev. A, 22 (1980) 1141.
[24] M. Pfeiffer, A. Lau and W. Wernecke, J. Raman Spectrosc., 15 (1984) 20.
[25] L. Ujj, A. Popp and G.H. Atkinson, Chem. Phys., 188 (1994) 221.
[26] R. Mathies, A.R. Oseroff and L. Stryer, Proc. Natl. Acad. Sci. USA, 73 (1976) 1.
[27] G.R. Loppnow and R.A. Mathies, Biophys. J., 54 (1988) 35.